Alcohol impacts an fMRI marker of neural inhibition in humans and rodents

Monami Nishio[1], Xinyi Wang[2], Eli J. Cornblath[3], Sung-Ho Lee[4], Yen-Yu Ian Shih[4], Nicola Palomero-Gallagher[5,6], Michael J. Arcaro[1], David M. Lydon-Staley[2,7], Allyson P. Mackey[1]*

[1] Department of Psychology, School of Arts and Sciences, University of Pennsylvania, Philadelphia, PA, USA
[2] Annenberg School for Communication, University of Pennsylvania, Philadelphia, PA, USA
[3] Department of Neurology, University of Pennsylvania, Perelman School of Medicine, University of Pennsylvania, Philadelphia, PA, USA
[4] Center for Animal MRI, University of North Carolina, Chapel Hill, NC, USA
[5] Institute of Medicine, Research Centre, Jülich, D-52425, Germany
[6] C. & O. Vogt Institute of Brain Research, Heinrich-Heine-University Düsseldorf, Düsseldorf, Germany
[7] Leonard Davis Institute of Health Economics, University of Pennsylvania, Philadelphia, PA, USA

Allyson Mackey
Email: mackeya@upenn.edu

Short title: Alcohol Alters fMRI Marker of Neural Inhibition

Author Contributions: M.N., D.M.L.-S. and A.P.M. conceptualized the study; X.W., E.C., S.H.L., Y.I.S and N.P.G collected data; M.N. analyzed the data and prepared the figures; M.N., M.J.A., D.M.L.-S. and A.P.M. interpreted the results; M.N. and A.P.M. wrote the manuscript; N.P.G, M.J.A., D.M.L.-S. and A.P.M. supervised M.N; all authors provided feedback on the manuscript.

Keywords: Hurst exponent; alcohol; neural inhibition; $GABA_A$ receptor; cross-species; rsfMRI

Abstract

Acute alcohol consumption leads to cognitive and behavioral disinhibition that increase health and social risks, such as traffic fatalities and violence. Although rodent studies have shown that alcohol affects neural inhibition, its relevance to humans remains largely unexplored. Here, we used the Hurst exponent—an fMRI-based marker of neural inhibition—to examine alcohol's effects in both rats and humans. In rats, acute alcohol administration significantly reduced the cortical Hurst exponent, suggesting decrease of neural inhibition. This reduction was strongly correlated with the spatial distribution of $GABA_A$ receptor expression, highlighting the key role of these receptors in mediating alcohol's effects. Similarly, in humans, acute alcohol consumption reduced the cortical Hurst exponent, especially in brain regions with high $GABA_A$ receptor expression. Our findings provide cross-species *in vivo* evidence that acute alcohol consumption modulates neural inhibition, offering new insights into the neural mechanisms underlying alcohol-induced behavioral modulation.

Introduction

Acute alcohol consumption triggers cognitive disinhibition, significantly increasing various health and social risks. For instance, approximately 37 people in the United States die daily in drunk-driving crashes, which account for 32% of all traffic fatalities (1). 40% of violent crimes, including assault, homicide, and domestic abuse, are committed by individuals with high blood alcohol content (BAC) at the time of their arrest (2). Moreover, nearly 30% of individuals who die by suicide consume alcohol shortly beforehand (3). In addition to causing cognitive impairment, acute alcohol intoxication disrupts motor coordination (4, 5) and affects the brain's reward systems (6–9), potentially leading to long-term issues such as binge drinking and addiction (10).

Cognitive disinhibition caused by acute alcohol are often associated with weakened top-down control (11). However, the precise mechanism by which alcohol affects cortical neuronal activity, leading to disrupted top-down control, remains unclear. *Ex vivo* studies using brain slices of rodents have shown that acute alcohol reduces the activity of excitatory neurons in the orbitofrontal (12, 13), cingulate (14), and prefrontal (15) cortices. An *in vivo* study using multielectrode extracellular recordings also reported decreased spike activity (15), while a separate study using calcium imaging found increased activity in pyramidal neurons in the prefrontal cortex (16). Fewer studies have examined alcohol's effects on inhibitory neurons. One *ex vivo* study showed that alcohol reduces the activity of fast-spiking interneurons in the prefrontal cortex (17). Similarly, an *in vivo* calcium imaging study observed suppressed activity of somatostatin interneurons in the same region (16). However, due to methodological limitations in brain region coverage, most of these studies have been conducted in prefrontal regions of rodents, and the effects of alcohol on other cortical areas remain largely unexplored.

The suppression of pyramidal neurons by alcohol is primarily attributed to its antagonistic effects on NMDA receptors, with minimal impact on AMPA receptor-mediated excitatory postsynaptic currents or $GABA_A$ receptor-mediated inhibitory postsynaptic currents (12, 14). On the other hand, several *ex vivo* studies using rodent brain slices have demonstrated that the agonistic effect on $GABA_A$ receptors is the primary mechanism through which alcohol affects inhibitory neurons (18–20). However, the situation is more complicated, as certain $GABA_A$ receptor subtypes are sensitive to alcohol at levels typically reached during social drinking, while other subtypes respond to higher concentrations associated with severe intoxication (21). Additionally, there is evidence that alcohol's impact on $GABA_A$ receptor activity is influenced by factors such as cell viability (22), cell type (23), and post-translational modifications like receptor phosphorylation (24, 25).

In humans, evidence of alcohol's effects on neural activity is limited and indirect. Some studies using arterial spin labeling have shown that alcohol increases cerebral blood flow across widespread cortical regions

(26–29). However, the relationship between neural activity and blood flow is complex and not fully understood (30–32). Other research has found that alcohol consumption increases functional connectivity (33–36), but this does not necessarily clarify the underlying neural mechanisms. Increased connectivity could result from various factors, including changes in neural activity—whether increased or decreased—or alcohol-induced vasoconstriction (32, 37, 38).

The Hurst exponent is a relatively new fMRI-based measure of neural inhibition (39–41). For a spectral density of the form $1/f^{\alpha}$, the Hurst exponent α measures the slope of the log-transformed spectral density and hence characterizes the power-law scaling of the amplitude fluctuations in various types of neuroimaging functional measures (42). Computational models have demonstrated that enhancing inhibition leads to an increase in the Hurst exponent of simulated local field potential and BOLD signals (39–41, 43). Using LFP data from mice, Gao et al. showed that regions with a higher GABA synapse density have a higher Hurst exponent, indicating a spatial relationship between the inhibitory synaptic density and the Hurst exponent (41). Lombardi further specified that a Hurst exponent of 1 corresponds to approximately 30% inhibitory synapses (43). Additionally, electrocorticography (ECoG) in macaques have shown that the Hurst exponent reflects changes in GABA activity induced by propofol, providing further evidence of a causal link between GABA and the Hurst exponent (41). The Hurst exponent is also influenced by excitatory neuronal signals. Trakoshis et al. showed that chemogenetically increasing pyramidal neuron excitability in the mouse prefrontal cortex lowered the Hurst exponent in BOLD signals (39). The Hurst exponent has been shown to be reduced in various mental disorders and related traits including ADHD (44), schizophrenia (45), and substance abuse (46), suggesting a decrease in neural inhibition. However, no study to date has pharmacologically validated the Hurst exponent as a marker of neural inhibition in humans. Alcohol exposure presents a rare opportunity to manipulate inhibitory neuronal activity in humans, making it a valuable tool for establishing a causal link between neural inhibition and the Hurst exponent. One pervious study applied 1/f neural noise — a measure similar to the Hurst exponent — to EEG to investigate the acute effects of alcohol but found no significant changes across the overall frequency ranges (47).

Applicable across species, the Hurst exponent overcomes species-specific limitations. For instance, relying solely on human data may be confounded by factors like alcohol-induced motion artifacts or cognitive slowing. Additionally, individual responses to alcohol vary widely due to factors such as genetic differences (48), sex (49), lean body mass (49), liver volume (49), stress levels (50), and drinking history (51). In contrast, relying exclusively on rodent data presents challenges related to anesthesia and translating findings to humans. Previous

acute alcohol studies have primarily focused on frontal regions in rodents, raising questions about their relevance to human brains and other cortical areas.

In this study, we first examine alcohol's impact on the Hurst exponent in genetically and environmentally consistent, alcohol-naive, and age-controlled rodents to minimize individual variability. We also explore the correlation between alcohol's effect on the Hurst exponent and $GABA_A$ receptor expression across the cortex, shedding light on the receptors likely contributing to alcohol's impact on neural inhibition. Next, we test the replicability of these findings in humans using an extensive repeated-measures (10 session) dataset. This study provides *in vivo* evidence of alcohol's effect on neural inhibition across species.

Methods and Materials

1. Rat data and analyses

1.1 Receptor expression

For the correlation analysis between alcohol effects and receptor expression, we used receptor autoradiographs generated in the framework of a study published by Palomero-Gallagher et al. (54, 55). Eight adult male LEW/Ztm rats were included in the study, with serial 20 µm coronal sections obtained at Bregma levels 4.20, 1.56, −2.76, and −4.80 (80). Sections were alternately stained for cell bodies using a modified silver Nissl-staining method or processed for quantitative *in vitro* autoradiography for receptor visualization. Receptor labeling involved pre-incubation in a Tris-citrate buffer to remove endogenous substances, incubation with [^{3}H]-flumazenil to identify total binding sites, and a rinsing step to stop the binding process. Flumazenil reveals the $GABA_A$-associated benzodiazepine ($GABA_A$/BZ) binding sites and is the ligand used the $GABA_A$ receptor in the receptor PET dataset published by Hansen et al. (59). Sections were exposed to beta-radiation-sensitive films alongside calibrated microscales to enable densitometric analysis of the ensuing receptor autoradiographs. The autoradiographs were digitized, their grey values converted into receptor densities (fmol/mg protein) by means of the microscales, and pseudo-color coded for visualization. Regions of interest (ROIs) were identified using the adjacent Nissl-stained sections, Bregma levels from the Paxinos and Watson rat brain atlas, and cortical parcellation by Haghir et al (56) to ensure precise boundaries, and manually annotated on the color-coded images. Receptor densities were extracted with AnaRec software(81), which extracted the receptor density measures from each ROI for further analysis.

126 1.2 In vivo Imaging subjects

127 A total of 38 Wistar rats bred and reared in-house were used in this experiment (breeders were purchased from
128 Envigo in Dublin, VA). On postnatal day (P) 1, litters (n = 21) were culled to 8–10 pups, with the same ratio
129 between sex whenever possible. The pups were housed with their mother until pair-housed at weaning (P21). The
130 rats were divided into two groups composed of both sexes. Each group was then used for the rs-fMRI at age P45
131 (n = 19, 11 females) or P80 (n = 19, 10 females). All animals were housed in a temperature- and humidity-
132 controlled vivarium on a 12:12 h light:dark cycle with ad libitum access to food and water.

133 1.3 Experimental design

134 Each animal underwent a single scanning session at the designated age (P45 or P80). A total of 75 min of blood
135 oxygenation level-dependent (BOLD) rs-fMRI data (five 15 min blocks) were acquired per single session. During
136 the rs-fMRI scan session, each animal was given a saline intraperitoneal injection after 15 min of the initial scan
137 (baseline), followed by two 1 g/kg and one 2 g/kg of 20% v/v ethanol injections (one injection for each 15 min
138 period) (10, 82). Rats were initially anesthetized with 4% isoflurane (Vaporizer #911103, VetEquip Inc.,
139 Livermore, CA, USA) mixed with medical air and endotracheally intubated using a 14G × 2"(P45) or 16G ×
140 2"(P45) intravenous (i.v.) catheter (Surflash Polyurethane Catheter, TERUMO, Somerset, NJ, USA). Respiration
141 was maintained by an MRI-compatible ventilator (MRI-1, CWE Inc, Ardmore, PA, USA) set at 60 breaths/min
142 and an inspiration time ratio of 40%. Next, the isoflurane concentration was adjusted to 2% and the animals were
143 secured to a custom-built, MR-compatible rat cradle. A rectal probe was used to monitor core body temperature
144 (OAKTON Temp9500, Cole-Parmer, Vernon Hills, IL, USA) and a capnometer was used to monitor heart rate,
145 peripheral blood oxygen saturation, and end-tidal CO2 (SURGIVET® V90041LF, Smith Medical, Dublin, OH,
146 USA). Body temperature was maintained at 37 ± 0.5 °C using a circulating water blanket connected to a
147 temperature adjustable water bath (Haake S13, Thermo Fisher Scientific, Waltham, MA, USA). Ventilation tidal
148 volume was adjusted to keep the heart rate at 300 ± 50 beats per minute, peripheral blood oxygen saturation above
149 96%, and end-tidal CO2 between 2.8 and 3.2%. End-tidal CO2 values from this capnometer system were
150 previously calibrated against an invasive sampling of arterial blood gas, reflecting a partial pressure of carbon
151 dioxide (pCO2) level of 30–40 mm Hg (83, 84). Upon stabilizing the animals, a cocktail of dexmedetomidine
152 (0.05 mg/kg/hr) and pancuronium bromide (0.5 mg/kg/hr) was continuously infused via the intraperitoneal cavity
153 (i.p.) (36, 85, 86) and the isoflurane was reduced to 0.5% (87). The infusion started 30 min prior to the rs-fMRI
154 scans (88).

155 1.4 MRI data acquisition

156 All MR images were collected through the UNC Center for Animal MRI (CAMRI) service on a Bruker BioSpec
157 9.4-Tesla, 30 cm bore system (Bruker BioSpin Corp., Billerica, MA) with ParaVision 6.0.1 on an AVANCE II
158 console and an RRI BFG 240/120 gradient insert (up to 1000 mT/m gradient strength; Resonance Research, Inc,
159 Billerica, MA) paired with a Prodrive BNG-500/1000 gradient amplifier (up to 500 A and 1000 V; Resonance
160 Research, Inc, Billerica, MA). All experiments used an 86 mm volume coil as the RF transmitter (Bruker BioSpin
161 Corp., Billerica, MA) and a 4-channel, rat brain array coil as the receiver (Bruker BioSpin Corp., Billerica, MA).
162 Magnetic field homogeneity was first optimized by global shimming, followed by local second-order shims using
163 a MAPSHIM protocol. The BOLD rs-fMRI data were acquired using a 2D multi-slice, single-shot, gradient-echo
164 EPI sequence: repetition time (TR) = 2000 ms, echo time (TE) = 14 ms bandwidth = 250 kHz, flip angle = 70°,
165 field of view (FOV) = 28.8 × 28.8 mm, matrix size = 72 × 72, slice number = 32, and slice thickness = 0.4 mm,
166 resulting in an isotropic voxel resolution of 0.4 mm.

167 1.5 MRI data preprocessing

168 All rs-fMRI data were first corrected for slice timing, followed by motion correction using AFNI (89). Each 4D
169 dataset was then averaged across time to improve signal-to-noise ratios (SNR) for subsequent skull stripping. The
170 brain mask for each time-averaged EPI image was estimated using an in-house developed 2D-UNET-based
171 machine learning algorithm (90) and was generated after manual refinement using ITK-snap (91). This mask was
172 subsequently applied to the corresponding rs-fMRI data to remove non-brain components. The skull-stripped data
173 were then spatially normalized to the in-house developed EPI template (52) using ANTs SyN diffeomorphic
174 registration (92) before further group-level analysis. For nuisance signal removal, third-degree polynomial curves
175 representing baseline trend and the six motion parameters estimated from motion correction were regressed out,
176 after which a 0.01–0.1 Hz band-pass filter was applied. The filtered data were then smoothed with a gaussian
177 kernel with a full width half maximum (FWHM) at 0.5 mm. Finally, the data was segmented into five blocks of
178 15 min scans to represent the brain state of each exposure period. The data-driven functional rat brain atlas (52)
179 was used for parcellation. Time-course data were averaged within the identified parcels for each subject and used
180 to calculate the Hurst exponent. The correspondence between these parcels and anatomical brain regions is
181 provided in Supplementary Table 3 of Lee et al., 2021 (52).

1.6 Hurst exponent

The Hurst exponent was calculated for each region for each run. The estimation of the Hurst exponent uses a discrete wavelet transform and a model of the time series as fractionally integrated processes (FIP) and is estimated using maximum likelihood estimation. FIP model was employed instead of the Fractional Gaussian Noise (fGn) model to eliminate the assumption of stationarity and the upper bound of H = 1. The FIP model provides greater flexibility and potentially increased sensitivity because it offers better estimation of between-subject variability, especially when estimates are close to or surpass H = 1. When H > 1, the time series is deemed non-stationary and displays long memory characteristics, such as being fractal. H is computed using the nonfractal MATLAB toolbox (https://github.com/wonsang/nonfractal)(28, 86). The specific function utilized is bfn_mfin_ml.m function with the 'filter' argument set to 'haar' and the 'ub' and 'lb' arguments set to [1.5,10] and [−0.5,0], respectively.

1.7 Alcohol effect modeling

To model the effect of alcohol, we employed a linear mixed-effects (LME) approach similar to that used in humans. For each brain region in the dataset, we constructed a model using the formula `Regional Hurst exponent ~ Run + Age + Sex + mean FD + (1 | Subject)`, where the run (saline, dose1, dose2, dose3), age, sex, and mean FD were treated as fixed effects. We selected the saline condition as the control instead of the baseline condition to eliminate the influence of the injection procedure on the Hurst exponent. Random intercepts were modeled for each subject to account for repeated measures. To calculate the alcohol effect for each brain region, we grouped the parcels belonging to each brain region and computed the average Hurst exponent of those parcels.

1.8 Correlation with $GABA_A$ receptor expression

For each parcel included in the functional rat brain atlas (52), we aggregated the $GABA_A$ receptor expression from the regions within the parcel and calculated their average. Consequently, receptor density data were available for 30 out of 50 parcels. We then computed the Pearson correlation between the alcohol effects and $GABA_A$ receptor expression for these 30 parcels.

2. Human data and analyses

2.1 Receptor expression

For the correlation analysis between alcohol effects and receptor expression, we used the dataset published by Hansen et al. (59). Volumetric PET images were collected for 19 different neurotransmitter receptors and

transporters across multiple studies. These images provide an estimate proportional to receptor densities, so we refer to the measured values (such as binding potential and tracer distribution volume) simply as receptor density. All PET images were registered to the MNI-ICBM 152 non-linear 2009 (version c, asymmetric) template and parcellated into 100 regions according to the Schaefer atlas.

2.2 Imaging participants

Participants meeting fMRI inclusion and study inclusion criteria (N = 11; M = 28.1 years, SD = 3.26 years; 4 women, 7 men; 3 identified as Asian, 5 identified as White, 1 identified as White and Hispanic or Latinx) were recruited. The study inclusion criteria was over the age of 21, have consumed at least 1 beverage containing alcohol during the 6 months before their first scan and have no physical conditions that could be influenced by drinking alcohol. The study's exclusion criteria included women who were pregnant, planning a pregnancy, or lactating. Individuals with a history of cancer, heart disease, stroke, or myocardial infarction within the past six months were also excluded. Participants with contraindications against fMRI, a history of problematic alcohol use (defined as an AUDIT score of 8 or higher), or liver disease were not eligible. Additionally, individuals taking medications for which alcohol use is contraindicated, as outlined by the National Institute on Alcohol Abuse and Alcoholism (NIAAA), were excluded from the study(93). All participants provided written informed consent. Procedures were approved by the University of Pennsylvania Institutional Review Board.

2.3 Experimental design

Participants attended one baseline survey visit and 10 laboratory visits where each session included surveys and an MRI session. At the start of each visit, participant first filled out a questionnaire including questions about their emotional state, sleep quality the night before, and most recent alcohol consumption. For 5 of the visits, participants were asked not to consume alcohol 12 hours before the visit and not to eat food for 3 hours prior to session. They were then provided with alcoholic beverages designed to increase their blood alcohol content (BAC) to 0.08% before they underwent MRI. The beverages consisted of vodka and orange juice mixed in a 3:1 juice:alcohol ratio. The amount consumed was equivalent to approximately 3 standard drinks of alcohol, though it was slightly more or less depending on the participant's age, gender, height, and weight as calculated through a BAC calculator (https://dionysus.psych.wisc.edu/open/bac_calc.html). Participants' BAC level was measured using a breathalyzer before and after the MRI scan. For the other 5 visits, participants were not provided with alcoholic beverages prior to the MRI scan. Among the 11 participants, one completed an additional non-alcohol session, resulting in a total of 5 alcohol and 6 non-alcohol sessions. One participant completed only five scans (2

alcohol and 3 non-alcohol sessions), and another completed only four scans (2 alcohol and 2 non-alcohol sessions). The two participants who did not complete all 10 sessions left the study because their eligibility for participating in the study changed (n = 1) and because they could no longer make time for the study (n = 1). The ordering of alcohol and non-alcohol sessions was randomized for each participant.

2.4 MRI data acquisition

Imaging data were acquired at University of Pennsylvania on a 3T Siemens Magnetom Prisma scanner equipped with a 32-channel head coil. High-resolution T1-weighted structural images were obtained using a multi-echo magnetisation-prepared rapid gradient-echo (MEMP-RAGE) sequence (repetition time (TR) = 2530 ms, echo time (TE) = 1.69/3.55/5.41/7.27 ms, TI = 1330 ms, FA (degree) = 7°, field of view (FoV) = 256 mm^2, voxel-size =1 mm^3, slice thickness = 1 mm, echo spacing = 11.1 ms, bandwidth = 650 Hz/pixel, and acquisition time = 5.26 min). During the structural scan, participants watched a 7-minute video featuring abstract shapes and moves in slow continuous transitions(94) in order to help reduce movement, boredom and nervousness. For rs-fMRI, 60 transversal slices were acquired by using an echoplanar imaging sequence (TR = 800 ms, TE = 30 ms, FA (degree) = 52°, field of view (FoV) = 216 mm^2, voxel-size = 2.4 mm^3, slice thickness = 2.4 mm, echo spacing = 0.51mm, bandwidth =2778 Hz/pixel, and acquisition time = 7.04 min). Each session included four resting-state scans with 2 fixation resting-state scans and 2 film clip resting-state scans. For this study, we only used the fixation resting-state scans. During these scans, a white fixation cross was presented on a black screen.

2.5 MRI data preprocessing

The T1-weighted (T1w) image underwent intensity nonuniformity correction using N4BiasFieldCorrection(95) from the Advanced Normalization ToolS (ANTS) version 2.2.0, and used as T1w reference throughout the workflow. Following this, skull stripping was performed using the antsBrainExtraction.sh script (ANTS version 2.2.0), with the OASIS template as the target. The brain mask was refined with a custom variation of the method to reconcile ANTS-derived and FreeSurfer (96) -derived segmentations of the cortical gray matter of Mindboggle (RRID:SCR_002438(97)). Spatial normalization to the ICBM 152 Nonlinear atlases version 2009c. (RRID:SCR_008796(98)) was performed through nonlinear registration with antsRegistration (ANTS, version 2.2.0, RRID:SCR_004757(99), using brain-extracted versions of both T1w volume and template. Brain tissue segmentation of CSF, white matter (WM), and gray matter was performed on the brain-extracted T1w using fast (Functional MRI of the Brain Software Library (FSL) version 5.0.9; RRID:SCR_002823(100)).

For each rs-fMRI run, a reference volume and its skull-stripped version were generated using a custom methodology of fMRIPrep version 20.2.0 (RRID:SCR_016216(101)), which is based on Nipype version 1.1.7 (RRID:SCR_002502(102), nipy/nipype:1.1.7). Brain surfaces were reconstructed using the recon-all command (96) before other processing, and reconstructed surfaces were used as input to fMRIprep. The BOLD reference was then coregistered to the T1w reference using bbregister (FreeSurfer), employing boundary-based registration(103). Coregistration was configured with nine degrees of freedom to account for distortions remaining in the BOLD reference. Head-motion parameters with respect to the BOLD reference (transformation matrices and six corresponding rotation and translation parameters) were estimated before any spatiotemporal filtering using the mcflirt tool (FSL version 5.0.9(104), and slice-time correction was performed using 3dTshift from AFNI 20160207 (RRID:SCR_005927(105)). The BOLD time series were resampled onto the MNIPediatricAsym standard space by applying a single, composite transform, generating a preprocessed BOLD run in MNI152NLin6Asym space.

Several confounding time series were calculated based on the preprocessed BOLD, including FD, DVARS (root-mean-square intensity difference from one volume to the next), and three region-wise global signals (CSF, WM, and the whole brain). FD and DVARS were calculated for each functional run, both using their implementations in Nipype(106). The head-motion estimates calculated in the correction step were also placed within the corresponding confounds file.

All resamplings can be performed with a single interpolation step by composing all the pertinent transformations (i.e., head-motion transform matrices and coregistrations to anatomic and template spaces). Gridded (volumetric) resamplings were performed using antsApplyTransforms (ANTS), configured with Lanczos interpolation to minimize the smoothing effects of other kernels (107).

Further preprocessing was performed using a confound regression procedure that has been optimized to reduce the influence of participant motion (108, 109); preprocessing was implemented in XCP-D 0.5.0 (108), a multimodal tool kit that deploys processing instruments from frequently used software libraries, including FSL(104) and AFNI(89). Further documentation is available at https://xcp-d.readthedocs.io/en/latest/ and https://github.com/PennLINC/xcp_d. Using XCP-D, the preprocessed functional time series on the fsLR cortical surface underwent nuisance regression, using a 36-parameter model that included three global signals (whole brain, CSF, and WM) and six motion parameters, as well as their derivatives, quadratic terms, and derivatives of quadratic terms. Linear regression, implemented in Scikit-Learn (0.24.2), was employed to regress the confounds. Motion censoring was applied, with outlier volumes exceeding FD = 0.3 mm flagged and removed from confound

regression. An interpolated version of the BOLD data is created by filling in the high-motion outlier volumes with cubic spline interpolated data, as implemented in *nilearn*. Any outlier volumes at the beginning or end of the run are replaced with the closest non-outlier volume's data, in order to avoid extrapolation by the interpolation function. If there was less than 100 seconds of data remaining after removing high-motion outlier volumes, those samples are excluded. No bandpass filtering was performed.

2.6 Hurst exponent

We used the same metrics as those applied to humans to calculate the Hurst exponent for rats.

2.7 Alcohol effect modeling

To model the effect of alcohol on the Hurst exponent, we employed a linear mixed-effects (LME) approach to account for the nested nature of the data (i.e., several runs nested in 11 participants) using the `lmer` function from the `lme4` package in R. For each brain region in the dataset, we constructed a model with the form `Regional Hurst exponent ~ Alcohol + psm_mean_fd + wps_mean_fd + Gender + (1 + Alcohol | Subject)`, where alcohol condition (alcohol / non-alcohol session), psm_mean_fd (person-average mean FD), wps_mean_fd (run-specific variation from the person-average mean FD), and gender were treated as fixed effects, while a random slope and intercept for alcohol were included for each subject to account for individual variability in the response to alcohol. The optimization was performed using the `optimx` method with the "nlminb" algorithm. For each region, we extracted the fixed effect of alcohol and calculated its significance through an ANOVA test. The p-values were then corrected for multiple comparisons using the false discovery rate (FDR) method.

2.8 Alignment with the S-A axis

We used the S-A axis derived by Sydnor and colleagues (31). This map encompasses various cortical hierarchies, including functional connectivity gradients, evolutionary cortical expansion patterns, anatomical ratios, allometric scaling, brain metabolism measures, perfusion indices, gene expression patterns, primary modes of brain function, cytoarchitectural similarity gradients, and cortical thickness.

2.9 Correlation with receptor expression

To calculate the correlation between alcohol's effect and $GABA_A$ receptor expression across the cortex, we computed the Pearson correlation across 100 cortical parcels. We compared the correlation coefficients and p-

values for the $GABA_A$ receptor and alcohol effect with those of other types of receptors to assess the specificity of the $GABA_A$ receptor in explaining the spatial distribution of alcohol's effect.

2.10 Spin-based spatial permutation testing

To address distance-dependent spatial autocorrelation in cortical data, we evaluated the significance of Pearson's correlations between two whole-brain cortical feature maps (the Hurst exponent) using non-parametric spin tests. These tests, also known as spatially constrained rotation tests, compare the observed correlation to a null distribution obtained by spatially iterating (spinning) one of the feature maps. Specifically, the null distribution is generated by rotating spherical projections of one map while preserving its spatial covariance structure. The *P* value (P_{spin}) is determined by comparing the empirical correlation to the distribution obtained from 10,000 spatial rotations. Spin tests were conducted using the spin permutation test algorithm available in the ENIGMA toolbox for Python (https://enigma-toolbox.readthedocs.io/en/latest/pages/08.spintest/index.html).

Results

Alcohol Exposure Reduces the Hurst Exponent in Rats.

We examined the effect of alcohol on the Hurst exponent in anesthetized rats. We parcellated the rat cortex into 50 parcels using the functional rat brain atlas (52). To calculate the Hurst exponent for each parcel, we applied the Fourier transform to the BOLD signal time series, computed the power spectral density (PSD), and estimated the slope of the best-fit line (Fig. 1A). Generally, neural signals and BOLD-fMRI data exhibit Hurst exponent values greater than 0.5, typically ranging between 0.6 and 0.9, indicating the presence of positive autocorrelation or persistent patterns in brain activity. A higher Hurst exponent, or a steeper slope, is believed to indicate greater neural inhibition (39–41). A total of 38 Wistar rats underwent a single scanning session, during which 75 minutes of resting-state fMRI (rs-fMRI) BOLD data were collected (five 15-minute blocks)(Fig. 1B). After the first 15 minutes (baseline), each rat received a saline injection, followed by two 1 g/kg and one 2 g/kg injections of 20% ethanol, with each injection administered at the start of the subsequent 15-minute periods. This protocol resulted in cumulative ethanol doses of 0, 1, 2, and 4 g/kg over the course of the scan. To focus on steady-state data, we excluded the first 5 minutes of each block containing the injection periods, analyzing only the final 10 minutes of each block.

Due to anesthesia, rat movement was generally minimal. However, three animals showed outlier levels of motion (mean framewise displacement exceeding 3 standard deviations above the mean) and were therefore excluded. After excluding these animals, there was a significant correlation between conditions (baseline, saline,

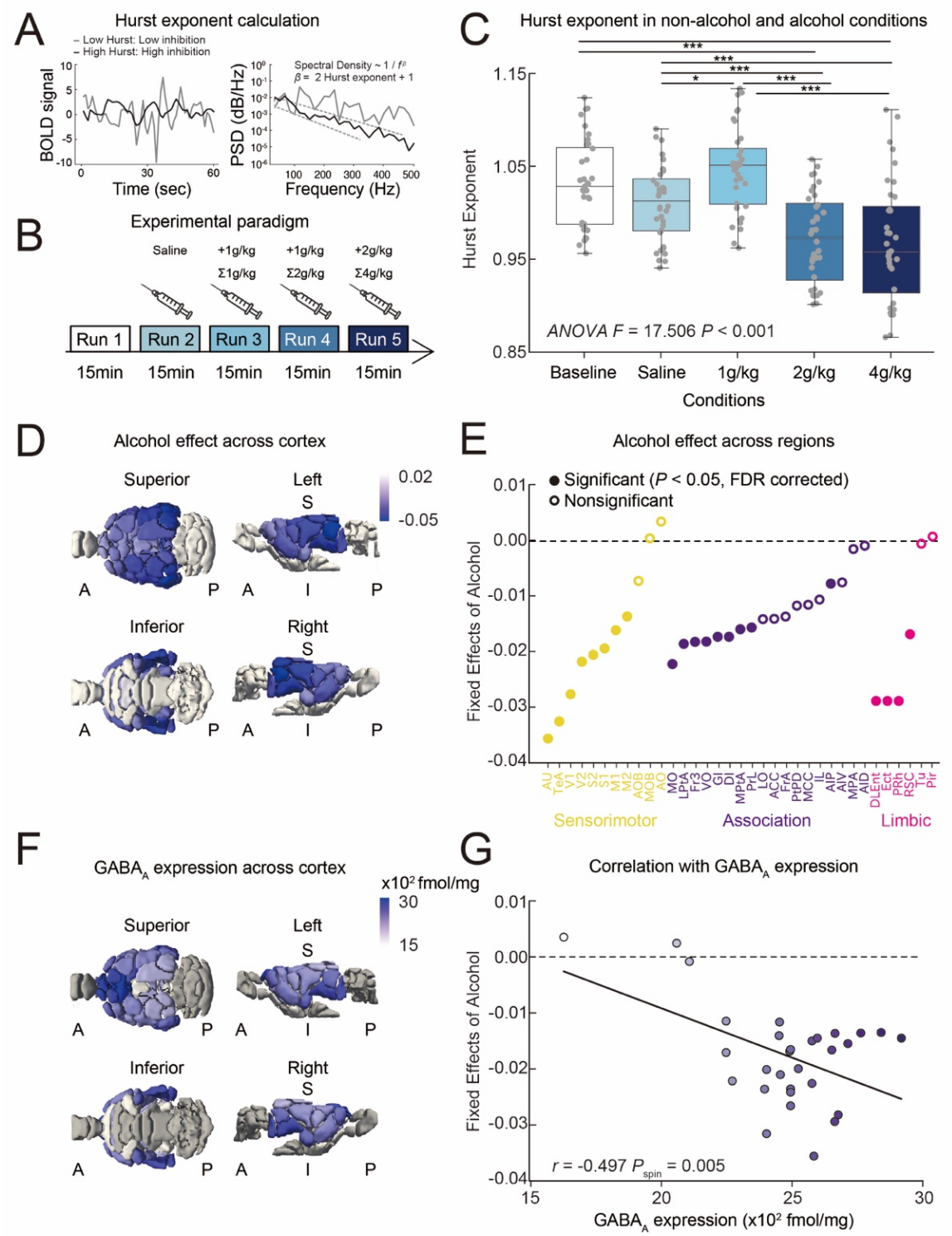

Figure 1. Alcohol's effect on the Hurst exponent in rats. (A) Examples of fMRI time series with high and low Hurst exponents and power spectrum densities (PSD). **(B)** Schematic illustration of the experimental paradigm for rats. **(C)** The whole-brain averaged Hurst exponent in rats under different conditions (ANOVA $F = 17.506$, $P < 0.001$). To control for motion, we regressed out the FD mean from the original Hurst values and added the residuals to the average Hurst exponent. Post-hoc Tukey HSD test $^{***}P < 0.001$, $^{**}P < 0.01$, $^{*}P < 0.05$. **(D)** Alcohol's effect across the cortex in rats. **(E)** Alcohol's effect in sensorimotor (yellow), association (purple) and limbic (pink) regions. Colored filled dots indicate regions with a significant alcohol effect that survived FDR correction, while unfilled dots represent regions with non-significant effects. The full names of the regions are listed in Table S1. **(F)** Cortical $GABA_A$ receptor expression as visualized *in vitro* by means of the radioligand [^{3}H] flumazenil. **(G)** Correlation between alcohol's effect and $GABA_A$ receptor expression across the cortex ($r = -0.497$, $P_{spin} = 0.005$).

352 and 1, 2, 4 g/kg alcohol) and mean framewise displacement (mean FD), suggesting that alcohol increases motion
353 (Fig. S1A, ANOVA $F = 4.576$, $P = 0.002$). There was no significant correlation between the Hurst exponent and
354 mean FD in any condition (Fig. S1B, Ps > 0.069). After the 2 g/kg and 4 g/kg ethanol injections, the Hurst
355 exponent was significantly lower compared to the first dose, saline, or baseline across the whole brain (Fig. 1C,
356 ANOVA $F = 17.506$, $P < 0.001$). We examined region-specific effects across 50 cortical parcellations defined by
357 the functional rat brain atlas (52) (Fig. 1D). The fixed effect of alcohol on the Hurst exponent was estimated using
358 a linear mixed-effects model for each parcel, where the dose of alcohol (0, 1,2,4 g/kg), age, sex, and mean FD
359 were treated as fixed effects. Random intercepts were modeled for each subject to account for repeated measures.
360 The fixed effect of alcohol was extracted and its significance was calculated through an ANOVA test. The p-
361 values was corrected for multiple comparisons using the false discovery rate (FDR) method. Since each brain
362 region covers multiple parcels, the mean fixed effect per region is calculated across these parcels. A brain region
363 was considered to have a significant effect if at least one parcel within the parcel survives FDR correction. The
364 effect of alcohol remained significant after FDR correction with $P < 0.05$ in many brain regions across sensory,
365 limbic, and association areas (Fig. 1E, the full names of the regions are listed in Table S1). The effect was
366 particularly strong in auditory regions (auditory cortex, temporal association cortex)(Fig. 1E).

367 Since previous research suggests that alcohol's effects on inhibitory neurons are primarily mediated
368 through $GABA_A$ receptors (18–20), we explored the correlation between alcohol's effect on the Hurst exponent
369 and $GABA_A$ receptor expression across the cortex. To quantify $GABA_A$ receptor density, we used *in vitro*
370 visualization with flumazenil, the most commonly used ligand in PET studies of the GABAergic system (53).
371 This analysis was conducted on rat brain data processed as part of a previously published study (54, 55).
372 Specifically, $GABA_A$ receptor expression was determined in cortical regions defined by the atlas proposed by
373 Haghir et al., 2024 (56). Out of the 50 regions of the functional rat brain atlas used in the fMRI study (52) , 30
374 regions have available receptor density data (Fig. 1F). The Pearson correlation between alcohol effects and
375 $GABA_A$ receptor expression was then calculated for these 30 parcels. The significance of the correlation was
376 assessed using spatially constrained rotation tests, known as 'spin tests' (57), because cortical data often exhibit
377 distance-dependent spatial autocorrelation potentially inflating the significance of correlations between two
378 cortical feature maps. There was a significant negative correlation between alcohol's effect on the Hurst exponent
379 and $GABA_A$ receptor expression (Fig. 1G, $r = -0.497$, $P_{spin} = 0.005$), indicating that regions with higher $GABA_A$
380 receptor expression experienced a greater reduction in the Hurst exponent. This result aligns with the previous
381 findings that alcohol's effect on inhibitory neurons is mainly mediated by $GABA_A$ receptors (18–20).

Subcortical regions also exhibited a significantly lower Hurst exponent after 2 g/kg or 4 g/kg ethanol injections (Fig. S2A, ANOVA $F = 9.109$, $P < 0.001$), with the amygdala (central amygdala, basolateral amygdala), cerebellum, and striatum (dorsal, dorsomedial and ventrolateral parts of caudate putamen) surviving FDR correction with $P < 0.05$ (Fig. S2B).

Alcohol Exposure Reduces the Hurst Exponent in Humans.

Since rodent models offer valuable insights into neural mechanisms but do not fully capture the complexities of human brain function, we next investigated whether similar effects occur in humans. Eleven healthy adults (ages 24–33 years) participated in the experiment. Of these, eight completed 10 laboratory sessions—five with alcohol and five without (Fig. 2A). One participant completed an additional non-alcohol session, resulting in a total of 5 alcohol and 6 non-alcohol sessions. One participant completed only five scans (2 alcohol and 3 non-alcohol

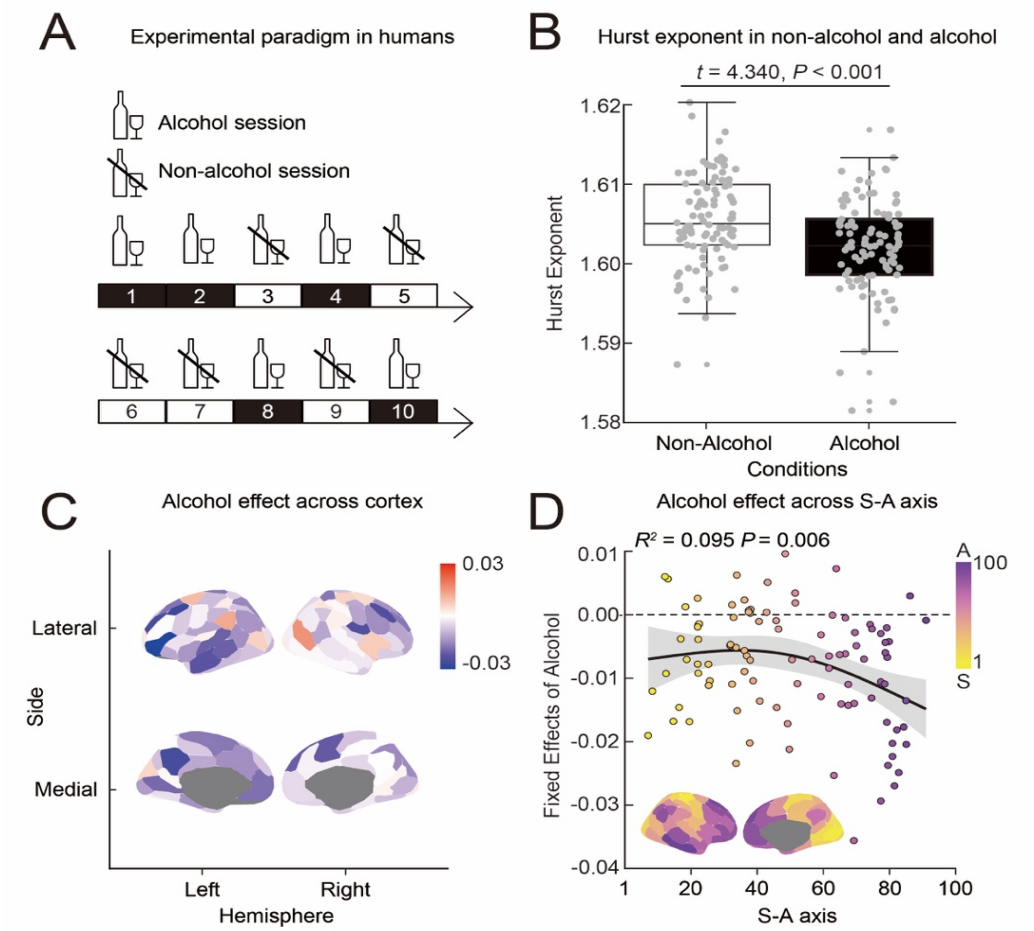

Figure 2. Alcohol's effect on the Hurst exponent in humans. (A) Schematic illustration of the experimental paradigms for humans. Healthy adults (ages 24–33) participated in 10 laboratory sessions—five with alcohol and five without. The order of alcohol and non-alcohol sessions was randomized. **(B)** The whole-brain averaged Hurst exponent in humans under non-alcohol (white) and alcohol (black) conditions ($t = 4.340$, $P < 0.001$). To control for motion, we regressed out the FD mean from the original Hurst values and added the residuals to the average Hurst exponent. **(C)** Alcohol's effect across the cortex. **(D)** Mapping of alcohol's effect along the sensory (yellow) -association (purple) axis ($R^2 = 0.095$, $P = 0.006$).

sessions), and another completed only four scans (2 alcohol and 2 non-alcohol sessions). During alcohol sessions, participants consumed alcoholic beverages designed to raise their blood alcohol content (BAC) to 0.08%, approximately equivalent to three standard drinks, before undergoing an MRI scan. In the non-alcohol sessions, participants did not consume alcohol prior to the MRI. The Hurst exponent was calculated from 7-minute runs of rs-fMRI data for both conditions. Since alcohol increased participant movement (Fig. S3A, $t = -3.677$, $P < 0.001$), particularly at moderate BAC levels (Fig. S3B), and the Hurst exponent significantly correlated with motion (Fig. S3C, Non-alcohol; $r = -0.811$, $P < 0.001$, Alcohol; $r = -0.814$, $P < 0.001$), we excluded sessions with a mean framewise displacement (mean FD) greater than 0.3 mm (Fig. S3C) and controlled for mean FD for subsequent analysis. We examined region-specific effects across 100 cortical parcellations defined by the Schaefer 100 atlas (58). The fixed effect of alcohol on the Hurst exponent was estimated using a linear mixed-effects (LME) model for each parcel, where alcohol condition (alcohol / non-alcohol session), person-average mean FD, run-specific variation from the person-average mean FD, and gender were treated as a fixed effects, while a random slope and intercept for alcohol was be included for each subject to model individual variability in the effect of alcohol on the hurst exponent.

Consistent with rodent findings, the average cortical Hurst exponent was significantly lower during alcohol sessions compared to non-alcohol sessions (Fig. 2B, $t = 4.340$, $P < 0.001$). This reduction remained significant using stricter motion exclusion criteria (mean FD < 0.2) (Fig. S3D, E, $t = 3.140$, $P = 0.002$). To assess regional specificity, we tested alcohol's effect on 100 evenly sized cortical parcels (28). Although no parcels survived FDR correction, the effect was consistently negative across the cortex (Fig. 2C). The most pronounced decreases were observed in association regions (Fig. 2D, GAM $R^2 = 0.095$, $P = 0.006$). This pattern remained even when non-alcohol sessions were subsampled to balance session counts between alcohol and non-alcohol sessions (Fig. S3F, R^2=0.063, P=0.029).

For the correlation analysis between alcohol's effects and receptor expression, we used the dataset published by Hansen et al., 2022 (59). Volumetric PET images were collected from multiple studies for 19 different neurotransmitter receptors, including $GABA_A$ receptors. These images provide an estimate proportional to receptor densities, so the measured values (such as binding potential and tracer distribution volume) are simply referred to as receptor density. All PET images were registered to the MNI-ICBM 152 non-linear 2009 (version c, asymmetric) template and parcellated into 100 parcels according to the Schaefer 100 atlas (58).

GABA$_A$ receptors were expressed throughout the cortex, with particularly strong expression at both ends of the S-A axis (Fig. 3A, B, $R^2 = 0.144$, $P < 0.001$). GABA$_A$ receptor expression significantly negatively correlated with alcohol's effect on the Hurst exponent, suggesting that regions with higher GABA$_A$ receptor expression experienced a greater reduction in the Hurst exponent due to alcohol. Since both alcohol's effects and GABA$_A$ receptor expression exhibit a significant correlation with the S-A axis (Fig. 2E, 3B), correlation between alcohol's effects and GABA$_A$ receptor expression could be partly explained by their independent associations with the S-A axis. However, the correlation between alcohol's effect and GABA$_A$ receptor expression remained significant even after controlling for the S-A axis with partial correlation test (Fig. 3C $r = -0.320$, $P = 0.001$), indicating that the S-A axis does not fully explain this relationship. Similarly, we examined the correlation between alcohol's

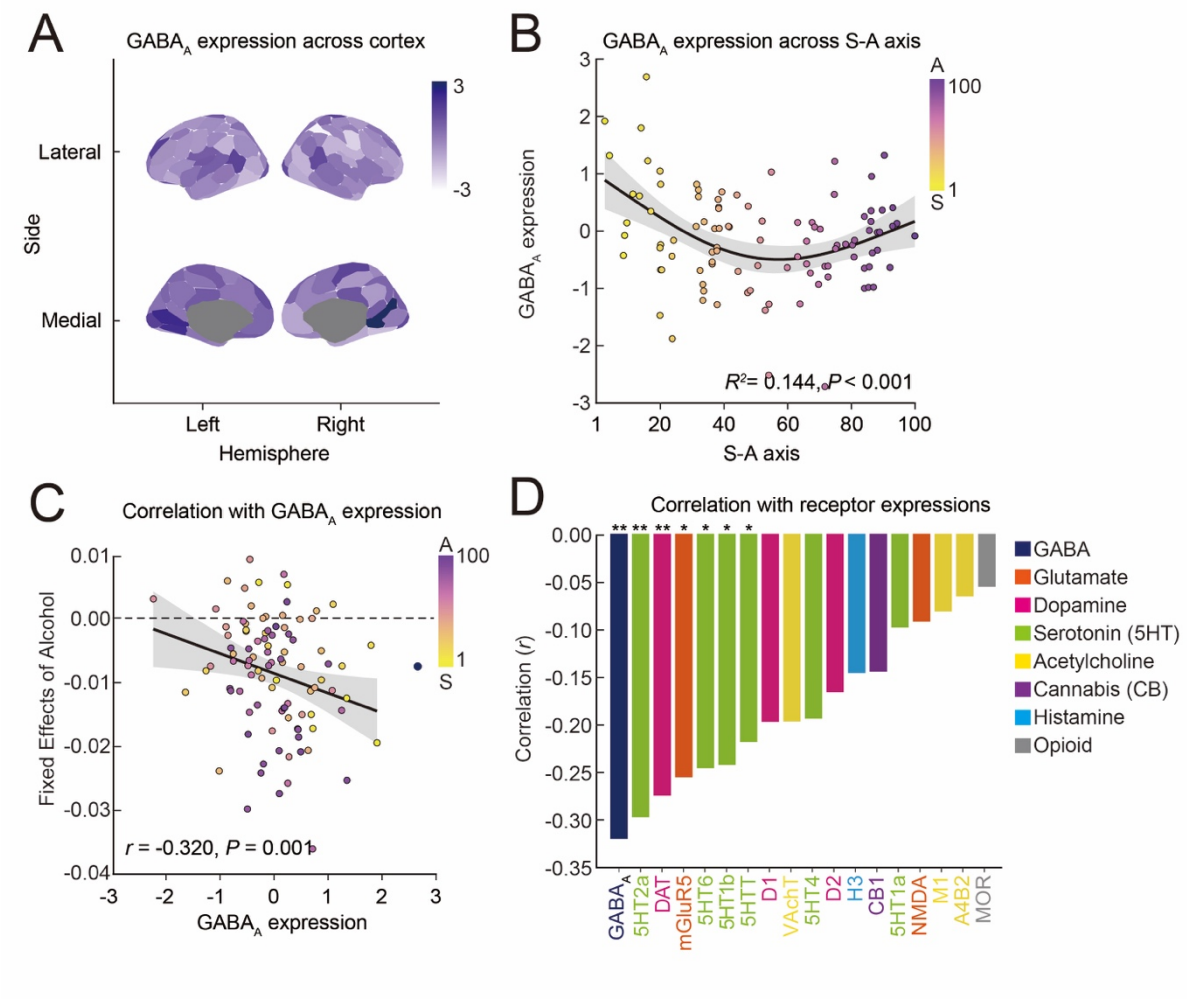

Figure 3. Alcohol's effect on the Hurst exponent in humans. (A) GABA$_A$ receptor expression across the cortex (z-scored). **(B)** Mapping of GABA$_A$ receptor expression along the sensory (yellow) -association (purple) axis ($R^2 = 0.144$, $P < 0.001$). **(C)** Correlation between alcohol's effect and GABA$_A$ receptor expression across the cortex. S-A rank is controlled using partial correlation test ($r = -0.320$, $P = 0.001$). **(D)** Comparison of correlation coefficients between group-averaged alcohol effect and different type of receptors. S-A rank is controlled using partial correlation test. $^{*}P < 0.05$, $^{**}P < 0.01$. The color of the bar indicates the type of receptor. Dark blue: GABA, Orange: Glutamate, Pink: Dopamine, Green: Serotonin (5HT), Yellow: Acetylcholine, Purple: Cannabis (CB), Light blue: Histamine, Gray: Opioid.

effect and the expression of various receptors, uptake sites and transporters while controlling for S-A axis. Among all, $GABA_A$ ranked the highest (Fig. 3D). Serotonergic receptors (5HT2A r = -0.297, P = 0.003, 5HT6 r = -0.246, P = 0.014, 5HT1b r = -0.243, P = 0.016, 5HTT r = -0.218, P = 0.030), dopamine transporter (DAT r = -0.275, P = 0.006), and metabotropic glutamate receptor 5 (mGluR5 r = -0.255, P = 0.011) also showed significant correlations with alcohol's effect.

Alcohol also significantly reduced the Hurst exponent in subcortical regions (Fig. S2C, t = 10.36, P < 0.001). Although no parcels survived FDR correction, the effect was most pronounced in the cerebellum, globus pallidus, nucleus accumbens, and substantia nigra (Fig. S2D).

Discussion

In this study, we investigated the effects of alcohol on the Hurst exponent—an fMRI-based marker of neural inhibition—in both rats and humans. Our findings revealed a consistent reduction in the Hurst exponent across species, indicating that alcohol decreases neural inhibition. Moreover, the spatial distribution of alcohol's effects was strongly correlated with $GABA_A$ receptor expression, underscoring their role in alcohol's effects on neural inhibition.

Most prior studies on alcohol's effects on cortical neuronal activities have focused on prefrontal regions in rodents (12–17), leaving its impact on other brain areas largely unexplored. Here, we demonstrated that alcohol's effects are widespread across the cortex. Studies using arterial spin labeling have similarly reported increased cerebral blood flow across broad cortical regions (26–29), suggesting alcohol's widespread impact on the cortex. Additionally, alcohol has been shown to enhance intrinsic connectivity within networks in the visual cortex (34, 60, 61), as well as in the sensorimotor cortex (34) and frontal cortex (33). Given the consistent reduction in the Hurst exponent within these sensorimotor and association areas, we speculate that decreased inhibition may lead to the disinhibition of excitatory neurons, increasing their spontaneous activity and potentially enhancing within-network connectivity. Interestingly, there are subtle differences in the spatial patterns of alcohol effects across species. In rats, the alcohol effect was strongest in sensory regions, while in humans, it was strongest in association regions. This could be due to differences in brain organization between species, with sensory regions being more dominant in rats and association regions playing a larger role in humans. Further studies are needed to explore the underlying mechanisms driving these species-specific effects.

Consistent with previous studies identifying $GABA_A$ receptors as key mediators of alcohol's effects on inhibitory neurons (18–20), we found a significant spatial correlation between alcohol's effects and $GABA_A$

459 receptor expression in both rodents and humans. However, there was considerable variability in the relationship
460 between $GABA_A$ receptor expression and alcohol effects in rats, as certain frontal regions—including the anterior
461 cingulate cortex, frontal association areas, prelimbic cortex, primary motor cortex (M1) and premotor cortex
462 (M2)—exhibited high $GABA_A$ receptor expression but only moderate reductions in the Hurst exponent following
463 alcohol exposure. This discrepancy may stem from variations in $GABA_A$ receptor subtypes, which have differing
464 sensitivities to alcohol (21–25). Additionally, in humans, we found that the serotonin 2A receptor (5HT2A) and
465 dopamine transporter (DAT) were strongly correlated with alcohol's effects ($P < 0.01$). Several studies have
466 confirmed an ethanol dose-dependent increase in dopamine release in both rodents and humans (6, 8, 9, 62–65).
467 Regions with high DAT expression, indicating dense dopamine innervation, are likely to be most affected by
468 alcohol-induced increases in dopamine. Since dopamine dose dependently suppresses inhibitory neuronal activity
469 through D2 receptors (66–68), these regions may experience a pronounced impact of alcohol on inhibitory
470 neuronal suppression. Alcohol is also known to interact with serotonin receptors (69–71). While the effects of
471 alcohol on excitatory neurons are primarily mediated via NMDA receptors (12, 14), we found no correlation
472 between alcohol's effects and NMDA receptor expression. Instead, we observed a significant correlation between
473 alcohol's effects and mGluR5. Both NMDA receptors and mGluR5 are closely localized on the cell surface, with
474 mGluR5 activation enhancing NMDA receptor activity (72–75). Therefore, it is possible that alcohol's effect on
475 the Hurst exponent could be influenced by its impact on excitatory neurons through mGluR5, which may, in turn,
476 modulate NMDA receptor activity.

477 We also observed a significant reduction in the Hurst exponent across several subcortical regions in rats,
478 as well as an overall effect in humans. Notably, a strong reduction in the Hurst exponent was observed in the
479 cerebellum and basal ganglia in both species. The reduction in inhibition and overactivation of Purkinje cells due
480 to the blockade of adenosine uptake in the cerebellum is known to cause motor dysfunction, referred to as ataxia,
481 which appears immediately after acute alcohol consumption (5). The alcohol-induced increase in striatal dopamine
482 release (50–56) is also possibly due to the suppression of inhibitory neurons and the subsequent overactivation of
483 dopamine neurons (7). Our findings of the reduced Hurst exponent in the cerebellum and basal ganglia align with
484 the known reduction of neural inhibition caused by alcohol. However, the validity of the Hurst exponent as a
485 marker of neural inhibition in subcortical regions remains uncertain, as no studies have yet applied this metric to
486 these areas. Additionally, the ROIs for subcortical regions varied significantly in size compared to the cortical
487 parcellations. Therefore, comparing the Hurst exponent across these regions should be done with caution.

While computational models and animal studies have suggested a causal link between the Hurst exponent and inhibitory neuronal activity (39–41), no studies had yet confirmed this relationship in humans. By leveraging alcohol exposure as a unique opportunity to directly manipulate inhibitory neuron activity in humans, we established a causal link between neural inhibition and the Hurst exponent. One challenge in using the Hurst exponent is its susceptibility to motion artifacts, particularly in conditions where motion differs significantly between conditions, such as in alcohol studies. Compared to rats, alcohol's effects on the Hurst exponent in humans were relatively subtle, as no individual cortical or subcortical regions showed significant effects after correction for multiple comparisons. This may be due to the strong correlation between motion and the Hurst exponent, as alcohol increases motion (presumable by reducing behavioral inhibition), and controlling for motion may have overly diminished the observed alcohol effect. Well-documented alcohol-induced changes in the cardiovascular system both in rodents and humans (76–78) could also contribute to increased motion, underscoring the need for better understanding and control of these factors.

Our study has several limitations. In rats, isoflurane anesthesia was used, which potentiates $GABA_A$ receptor function. Although anesthesia conditions were consistent between alcohol and non-alcohol sessions, and our results aligned with findings from awake human participants, it remains possible that anesthesia interacted with alcohol's effects in rodents. Replicating our findings in awake rodents or under different anesthesia types would strengthen these conclusions. Furthermore, some animal studies suggest that alcohol's effects on inhibitory neuronal activity are dose-dependent (16) Consistent with this, we observed dose-dependent effects on the Hurst exponent in rats. Specifically, 1 g/kg did not cause a significant change, whereas 2 g/kg and 4 g/kg significantly reduced the Hurst exponent. Our study used a blood alcohol concentration of 0.08% in humans, which is the legal driving limit and considered relatively high. Our findings may differ at lower doses; therefore, future research should investigate these dose-dependent effects in humans. Finally, to enhance statistical power in our group-level analysis with a relatively small sample size, we used a repeated-measures design. While this approach is appropriate for estimating main effects of alcohol, the sample size was not large enough for investigating between-individual variability, such as differences related to gender, age, or genetic background.

In summary, this study provides *in vivo* evidence of alcohol's suppressive effects on neural inhibition across species. Given that most alcohol studies are conducted in rodents, the use of consistent methods across species and the consistency of our cross-species findings may be critical for future translational research (79). These insights could be valuable in informing clinical interventions and preventive strategies to address the health risks associated with alcohol consumption.

Acknowledgements

We thank all of the individuals who participated in this research. This study was supported by a National Science Foundation CAREER award (to A.P.M. under Grant No. 2045095), Brain & Behavior Research Foundation (to D.M.L.-S.), Quad Fellowship (to M.N.) and Nakajima Foundation Scholarship (to M.N.).

Disclosures

The authors declare no competing interests.

526 **References**

527 1. National Highway Traffic Safety Administration, "Drunk Driving" (2022).
528 2. K. V. Sontate, *et al.*, Alcohol, Aggression, and Violence: From Public Health to Neuroscience. *Front*
529 *Psychol* **12** (2021).
530 3. Christine Moutier, "Suicidal Behavior" (2023).
531 4. M. Saeed Dar, Ethanol-induced cerebellar ataxia: Cellular and molecular mechanisms. *Cerebellum* **14**
532 (2015).
533 5. H. Mitoma, M. Manto, A. G. Shaikh, Mechanisms of ethanol-induced cerebellar ataxia: Underpinnings
534 of neuronal death in the cerebellum. *Int J Environ Res Public Health* [Preprint] (2021).
535 6. I. Boileau, *et al.*, Alcohol promotes dopamine release in the human nucleus accumbens. *Synapse* **49**
536 (2003).
537 7. K. Charlet, A. Beck, A. Heinz, The dopamine system in mediating alcohol effects in humans. *Curr Top*
538 *Behav Neurosci* **13** (2011).
539 8. K. Yoshimoto, W. J. McBride, L. Lumeng, T. K. Li, Alcohol stimulates the release of dopamine and
540 serotonin in the nucleus accumbens. *Alcohol* **9** (1992).
541 9. N. B. L. Urban, *et al.*, Sex differences in striatal dopamine release in young adults after oral alcohol
542 challenge: A positron emission tomography imaging study with [11C]raclopride. *Biol Psychiatry* **68**
543 (2010).
544 10. T. A. Shnitko, L. P. Spear, D. L. Robinson, Adolescent binge-like alcohol alters sensitivity to acute
545 alcohol effects on dopamine release in the nucleus accumbens of adult rats. *Psychopharmacology (Berl)*
546 **233** (2016).
547 11. C. Fernando Valenzuela, Alcohol and neurotransmitter interactions. *Alcohol Research and Health* **21**
548 (1997).
549 12. K. A. Badanich, P. J. Mulholland, J. T. Beckley, H. Trantham-Davidson, J. J. Woodward, Ethanol
550 reduces neuronal excitability of lateral orbitofrontal cortex neurons via a glycine receptor dependent
551 mechanism. *Neuropsychopharmacology* **38** (2013).
552 13. S. Nimitvilai, *et al.*, Orbitofrontal neuroadaptations and cross-species synaptic biomarkers in heavy-
553 drinking macaques. *Journal of Neuroscience* **37** (2017).
554 14. Q. Li, W. A. Wilson, H. Scott Swartzwelder, Differential effect of ethanol on NMDA EPSCs in
555 pyramidal cells in the posterior cingulate cortex of juvenile and adult rats. *J Neurophysiol* **87** (2002).
556 15. Y. Tu, *et al.*, Ethanol inhibits persistent activity in prefrontal cortical neurons. *Journal of Neuroscience*
557 **27** (2007).
558 16. M. Li, *et al.*, Alcohol reduces the activity of somatostatin interneurons in the mouse prefrontal cortex: A
559 neural basis for its disinhibitory effect? *Neuropharmacology* **188** (2021).
560 17. J. J. Woodward, M. J. Pava, Effects of ethanol on persistent activity and up-states in excitatory and
561 inhibitory neurons in prefrontal cortex. *Alcohol Clin Exp Res* **33** (2009).
562 18. M. R. Diaz, C. F. Valenzuela, Sensitivity of GABAergic Tonic Currents to Acute Ethanol in Cerebellar
563 Granule Neurons is Not Age- or δ Subunit-Dependent in Developing Rats. *Alcohol Clin Exp Res* **40**
564 (2016).
565 19. J. Liang, *et al.*, Chronic intermittent ethanol-induced switch of ethanol actions from extrasynaptic to
566 synaptic hippocampal GABAA receptors. *Journal of Neuroscience* **26** (2006).
567 20. F. Jia, D. Chandra, G. E. Homanics, N. L. Harrison, Ethanol modulates synaptic and extrasynaptic
568 GABAA receptors in the thalamus. *Journal of Pharmacology and Experimental Therapeutics* **326**
569 (2008).
570 21. S. Kumar, *et al.*, The role of GABAA receptors in the acute and chronic effects of ethanol: A decade of
571 progress. *Psychopharmacology (Berl)* **205** (2009).
572 22. L. Aguayo, R. Peoples, H. Yeh, G. Yevenes, GABA-A Receptors as Molecular Sites of Ethanol Action.
573 Direct or Indirect Actions? *Curr Top Med Chem* **2** (2005).
574 23. D. W. Sapp, H. H. Yeh, Ethanol-GABA(A) receptor interactions: A comparison between cell lines and
575 cerebellar Purkinje cells. *Journal of Pharmacology and Experimental Therapeutics* **284** (1998).

24. R. A. Harris, *et al.*, Mutant mice lacking the γ isoform of protein kinase C show decreased behavioral actions of ethanol and altered function of γ-aminobutyrate type A receptors. *Proc Natl Acad Sci U S A* **92** (1995).
25. B. Förstera, P. A. Castro, G. Moraga-Cid, L. G. Aguayo, Potentiation of gamma aminobutyric acid receptors (GABAAR) by ethanol: How are inhibitory receptors affected? *Front Cell Neurosci* **10** (2016).
26. N. M. Strang, *et al.*, Dose-dependent effects of intravenous alcohol administration on cerebral blood flow in young adults. *Psychopharmacology (Berl)* **232** (2015).
27. E. Rickenbacher, D. N. Greve, S. Azma, J. Pfeuffer, K. Marinkovic, Effects of alcohol intoxication and gender on cerebral perfusion: An arterial spin labeling study. *Alcohol* **45** (2011).
28. M. Marxen, *et al.*, Acute effects of alcohol on brain perfusion monitored with arterial spin labeling magnetic resonance imaging in young adults. *Journal of Cerebral Blood Flow and Metabolism* **34** (2014).
29. R. J. Mathew, W. H. Wilson, Regional cerebral blood flow changes associated with ethanol intoxication. *Stroke* **17** (1986).
30. B. Stefanovic, J. M. Warnking, G. B. Pike, Hemodynamic and metabolic responses to neuronal inhibition. *Neuroimage* **22** (2004).
31. B. M. Katz, L. R. Walton, K. M. Houston, D. H. Cerri, Y. Y. I. Shih, Putative neurochemical and cell type contributions to hemodynamic activity in the rodent caudate putamen. *Journal of Cerebral Blood Flow and Metabolism* [Preprint] (2023).
32. D. H. Cerri, *et al.*, Distinct neurochemical influences on fMRI response polarity in the striatum. *Nat Commun* **15** (2024).
33. J. Han, S. Keedy, C. H. Murray, S. Foxley, H. de Wit, Acute effects of alcohol on resting-state functional connectivity in healthy young men. *Addictive Behaviors* **115** (2021).
34. R. Ochi, *et al.*, Patterns of functional connectivity alterations induced by alcohol reflect somatostatin interneuron expression in the human cerebral cortex. *Sci Rep* **12** (2022).
35. S. H. Lee, *et al.*, Acute alcohol induces greater dose-dependent increase in the lateral cortical network functional connectivity in adult than adolescent rats. *Addiction Neuroscience* **7** (2023).
36. M. A. Broadwater, *et al.*, Adolescent alcohol exposure decreases frontostriatal resting-state functional connectivity in adulthood. *Addiction Biology* **23** (2018).
37. F. Rocchi, *et al.*, Increased fMRI connectivity upon chemogenetic inhibition of the mouse prefrontal cortex. *Nat Commun* **13** (2022).
38. W. T. Zhang, *et al.*, Spectral fiber photometry derives hemoglobin concentration changes for accurate measurement of fluorescent sensor activity. *Cell Reports Methods* **2** (2022).
39. S. Trakoshis, *et al.*, Intrinsic excitation-inhibition imbalance affects medial prefrontal cortex differently in autistic men versus women. *Elife* **9** (2020).
40. M. Chini, T. Pfeffer, I. Hanganu-Opatz, An increase of inhibition drives the developmental decorrelation of neural activity. *Elife* **11** (2022).
41. R. Gao, E. J. Peterson, B. Voytek, Inferring synaptic excitation/inhibition balance from field potentials. *Neuroimage* **158** (2017).
42. K. Linkenkaer-Hansen, V. V. Nikouline, J. M. Palva, R. J. Ilmoniemi, Long-range temporal correlations and scaling behavior in human brain oscillations. *Journal of Neuroscience* **21** (2001).
43. F. Lombardi, H. J. Herrmann, L. de Arcangelis, Balance of excitation and inhibition determines 1/f power spectrum in neuronal networks. *Chaos* **27** (2017).
44. A. J. Stier, *et al.*, A pattern of cognitive resource disruptions in childhood psychopathology. *Network Neuroscience* **7** (2023).
45. M. O. Sokunbi, *et al.*, Nonlinear complexity analysis of brain fMRI signals in schizophrenia. *PLoS One* **9** (2014).
46. J. S. Ide, S. Hu, S. Zhang, L. R. Mujica-Parodi, C. S. R. Li, Power spectrum scale invariance as a neural marker of cocaine misuse and altered cognitive control. *Neuroimage Clin* **11** (2016).
47. A. K. Stock, M. Pertermann, M. Mückschel, C. Beste, High-dose ethanol intoxication decreases 1/f neural noise or scale-free neural activity in the resting state. *Addiction Biology* **25** (2020).

48. H. J. Edenberg, The genetics of alcohol metabolism: Role of alcohol dehydrogenase and aldehyde dehydrogenase variants. *Alcohol Research and Health* **30** (2007).
49. V. Vatsalya, N. D. Byrd, B. L. Stangl, R. Momenan, V. A. Ramchandani, Influence of age and sex on alcohol pharmacokinetics and subjective pharmacodynamic responses following intravenous alcohol exposure in humans. *Alcohol* **107** (2023).
50. R. Sinha, Alcohol's Negative Emotional Side: The Role of Stress Neurobiology in Alcohol Use Disorder. *Alcohol Res* **42** (2022).
51. P. Follesa, *et al.*, Neurosteroids, GABAA receptors, and ethanol dependence. *Psychopharmacology (Berl)* **186** (2006).
52. S. H. Lee, *et al.*, An isotropic EPI database and analytical pipelines for rat brain resting-state fMRI. *Neuroimage* **243** (2021).
53. J. D. Andersson, D. Matuskey, S. J. Finnema, Positron emission tomography imaging of the γ-aminobutyric acid system. *Neurosci Lett* [Preprint] (2019).
54. N. Palomero-Gallagher, *et al.*, Receptor fingerprinting the circling ci2 rat mutant: Insights into brain asymmetry and motor control. *Exp Neurol* **210** (2008).
55. N. Palomero-Gallagher, A. A. Schleicher, K. Zilles, W. Löscher, The circling ci2 rat mutant revisited: Receptor architecture of the motor cortex. *Neuroscience* **170** (2010).
56. H. Haghir, A. Kuckertz, L. Zhao, J. Hami, N. Palomero-Gallagher, A new map of the rat isocortex and proisocortex: cytoarchitecture and M2 receptor distribution patterns. *Brain Struct Funct* (2023). https://doi.org/10.1007/s00429-023-02654-7.
57. A. F. Alexander-Bloch, *et al.*, On testing for spatial correspondence between maps of human brain structure and function. *Neuroimage* **178** (2018).
58. A. Schaefer, *et al.*, Local-Global Parcellation of the Human Cerebral Cortex from Intrinsic Functional Connectivity MRI. *Cerebral Cortex* **28** (2018).
59. J. Y. Hansen, *et al.*, Mapping neurotransmitter systems to the structural and functional organization of the human neocortex. *Nat Neurosci* **25** (2022).
60. N. Khalili-Mahani, *et al.*, Effects of morphine and alcohol on functional brain connectivity during "resting state": A placebo-controlled crossover study in healthy young men. *Hum Brain Mapp* **33** (2012).
61. F. Esposito, *et al.*, Alcohol increases spontaneous BOLD signal fluctuations in the visual network. *Neuroimage* **53** (2010).
62. H. J. Yim, R. A. Gonzales, Ethanol-induced increases in dopamine extracellular concentration in rat nucleus accumbens are accounted for by increased release and not uptake inhibition. *Alcohol* **22** (2000).
63. Q. S. Yan, Extracellular dopamine and serotonin after ethanol monitored with 5- minute microdialysis. *Alcohol* **19** (1999).
64. H. J. Yim, T. Schallert, P. K. Randall, R. A. Gonzales, Comparison of local and systemic ethanol effects on extracellular dopamine concentration in rat nucleus accumbens by microdialysis in *Alcoholism: Clinical and Experimental Research*, (1998).
65. S. Aalto, *et al.*, Intravenous ethanol increases dopamine release in the ventral striatum in humans: PET study using bolus-plus-infusion administration of [11 C]raclopride. *Journal of Perinatology* **35** (2015).
66. C. Le Moine, P. Gaspar, Subpopulations of cortical GABAergic interneurons differ by their expression of D1 and D2 dopamine receptor subtypes. *Molecular Brain Research* **58** (1998).
67. H. Trantham-Davidson, L. C. Neely, A. Lavin, J. K. Seamans, Mechanisms underlying differential D1 versus D2 dopamine receptor regulation of inhibition in prefrontal cortex. *Journal of Neuroscience* **24** (2004).
68. N. Gorelova, J. K. Seamans, C. R. Yang, Mechanisms of dopamine activation of fast-spiking interneurons that exert inhibition in rat prefrontal cortex. *J Neurophysiol* **88** (2002).
69. D. M. Lovinger, Q. Zhou, Alcohols potentiate ion current mediated by recombinant 5-HT3RA receptors expressed in a mammalian cell line. *Neuropharmacology* **33** (1994).
70. D. M. Lovinger, R. W. Peoples, "Actions of Alcohols and other Sedative/Hypnotic Compounds on Cation Channels Associated with Glutamate and 5-HT3 Receptors" in *Alcohol, Cell Membranes, and Signal Transduction in Brain*, (1993).

71. D. M. Lovinger, Serotonin's role in alcohol's effects on the brain. *Alcohol Research and Health* **21** (1997).
72. D. Z. Jin, B. Xue, L. M. Mao, J. Q. Wang, Metabotropic glutamate receptor 5 upregulates surface NMDA receptor expression in striatal neurons via CaMKII. *Brain Res* **1624** (2015).
73. A. Pisani, *et al.*, Metabotropic glutamate receptor 5 mediates the potentiation of N-methyl-D-aspartate responses in medium spiny striatal neurons. *Neuroscience* **106** (2001).
74. S. Attucci, V. Carlá, G. Mannaioni, F. Moroni, Activation of type 5 metabotropic glutamate receptors enhances NMDA responses in mice cortical wedges. *Br J Pharmacol* **132** (2001).
75. H. Awad, G. W. Hubert, Y. Smith, A. I. Levey, P. J. Conn, Activation of metabotropic glutamate receptor 5 has direct excitatory effects and potentiates NMDA receptor currents in neurons of the subthalamic nucleus. *Journal of Neuroscience* **20** (2000).
76. M. R. Piano, Alcohol's effects on the cardiovascular system. *Alcohol Res* **38** (2017).
77. S. Brunner, *et al.*, Impact of acute ethanol intake on cardiac autonomic regulation. *Sci Rep* **11** (2021).
78. D. L. Lucas, R. A. Brown, M. Wassef, T. D. Giles, Alcohol and the cardiovascular system: Research challenges and opportunities. *J Am Coll Cardiol* **45** (2005).
79. M. Fritz, A. M. Klawonn, N. M. Zahr, Neuroimaging in alcohol use disorder: From mouse to man. *J Neurosci Res* **100** (2022).
80. G. Paxinos, C. Watson, The Rat Brain in Stereotaxic Coordinates Seventh Edition. *Elsevier Academic Press* **170** (2014).
81. D. Impieri, *et al.*, Receptor density pattern confirms and enhances the anatomic-functional features of the macaque superior parietal lobule areas. *Brain Struct Funct* **224** (2019).
82. T. A. Shnitko, L. C. Kennerly, L. P. Spear, D. L. Robinson, Ethanol reduces evoked dopamine release and slows clearance in the rat medial prefrontal cortex. *Alcohol Clin Exp Res* **38** (2014).
83. Y. Y. I. Shih, *et al.*, Endogenous opioid-dopamine neurotransmission underlie negative CBV fMRI signals. *Exp Neurol* **234** (2012).
84. Y. Y. I. Shih, *et al.*, Ultra high-resolution fMRI and electrophysiology of the rat primary somatosensory cortex. *Neuroimage* **73** (2013).
85. D. L. Albaugh, *et al.*, Functional Magnetic Resonance Imaging of Electrical and Optogenetic Deep Brain Stimulation at the Rat Nucleus Accumbens. *Sci Rep* **6** (2016).
86. C. P. Pawela, *et al.*, A protocol for use of medetomidine anesthesia in rats for extended studies using task-induced BOLD contrast and resting-state functional connectivity. *Neuroimage* **46** (2009).
87. M. Fukuda, A. L. Vazquez, X. Zong, S. G. Kim, Effects of the α2-adrenergic receptor agonist dexmedetomidine on neural, vascular and BOLD fMRI responses in the somatosensory cortex. *European Journal of Neuroscience* **37** (2013).
88. H. Lu, *et al.*, Rat brains also have a default mode network. *Proc Natl Acad Sci U S A* **109** (2012).
89. R. W. Cox, AFNI: Software for analysis and visualization of functional magnetic resonance neuroimages. *Computers and Biomedical Research* **29** (1996).
90. L. M. Hsu, *et al.*, Automatic Skull Stripping of Rat and Mouse Brain MRI Data Using U-Net. *Front Neurosci* **14** (2020).
91. P. A. Yushkevich, *et al.*, User-guided 3D active contour segmentation of anatomical structures: Significantly improved efficiency and reliability. *Neuroimage* **31** (2006).
92. B. B. Avants, C. L. Epstein, M. Grossman, J. C. Gee, Symmetric diffeomorphic image registration with cross-correlation: Evaluating automated labeling of elderly and neurodegenerative brain. *Med Image Anal* **12** (2008).
93. National Institute on Alcohol Abuse and Alcoholism, Alcohol's Effects on Health: Research-based Information on Drinking and It's Impact. *National Institute on Alcohol Abuse and Alcoholism* (2022).
94. T. Vanderwal, C. Kelly, J. Eilbott, L. C. Mayes, F. X. Castellanos, Inscapes: A movie paradigm to improve compliance in functional magnetic resonance imaging. *Neuroimage* **122** (2015).
95. N. J. Tustison, *et al.*, N4ITK: Improved N3 bias correction. *IEEE Trans Med Imaging* **29** (2010).
96. A. M. Dale, B. Fischl, M. I. Sereno, Cortical surface-based analysis: I. Segmentation and surface reconstruction. *Neuroimage* **9** (1999).
97. A. Klein, *et al.*, Mindboggling morphometry of human brains. *PLoS Comput Biol* **13** (2017).

98. V. Fonov, *et al.*, Unbiased average age-appropriate atlases for pediatric studies. *Neuroimage* **54** (2011).
99. B. B. Avants, *et al.*, The optimal template effect in hippocampus studies of diseased populations. *Neuroimage* **49** (2010).
100. Y. Zhang, M. Brady, S. Smith, Segmentation of brain MR images through a hidden Markov random field model and the expectation-maximization algorithm. *IEEE Trans Med Imaging* **20** (2001).
101. O. Esteban, *et al.*, fMRIPrep: a robust preprocessing pipeline for functional MRI. *Nat Methods* **16** (2019).
102. K. J. Gorgolewski, *et al.*, The brain imaging data structure, a format for organizing and describing outputs of neuroimaging experiments. *Sci Data* **3** (2016).
103. D. N. Greve, B. Fischl, Accurate and robust brain image alignment using boundary-based registration. *Neuroimage* **48** (2009).
104. M. Jenkinson, P. Bannister, M. Brady, S. Smith, Improved optimization for the robust and accurate linear registration and motion correction of brain images. *Neuroimage* **17** (2002).
105. R. W. Cox, J. S. Hyde, Software tools for analysis and visualization of fMRI data. *NMR Biomed* **10** (1997).
106. J. D. Power, *et al.*, Methods to detect, characterize, and remove motion artifact in resting state fMRI. *Neuroimage* **84** (2014).
107. C. Lanczos, Evaluation of Noisy Data. *Journal of the Society for Industrial and Applied Mathematics Series B Numerical Analysis* **1** (1964).
108. R. Ciric, *et al.*, Mitigating head motion artifact in functional connectivity MRI. *Nat Protoc* **13** (2018).
109. T. D. Satterthwaite, *et al.*, Impact of puberty on the evolution of cerebral perfusion during adolescence. *Proc Natl Acad Sci U S A* **111** (2014).

755 **Supplementary Table 1. Full names of the brain regions**

	Acronym	Full name
Rat cortical regions	AU	auditory cortex
	TeA	temporal association cortex
	V1/V2	visual cortices - primary / secondary
	S1/S2	somatosensory cortices - primary / secondary
	M1/M2	motor cortices - primary / secondary
	AOB/MOB	olfactory bulb - accessory / main
	AO	anterior olfactory area
	MO/VO/LO	orbital corticies - medial / ventral / lateral
	MPtA/LPtA	parietal association cortex- medial / lateral
	GI/DI	insular cortices - granular / dysgranular
	AID/AIV/AIP	insular cortices - dorsal / ventral / posterior agranular
	PrL/IL	medial prefrontal cortex - prelimbic / infralimbic
	Fr3	frontal cortex, area 3
	FrA	frontal association cortex
	ACC/MCC	cingulate cortices - anterior / mid
	MPA	medial preoptic area
	Ect/PRh/DLEnt	rhinal cortices - ectp / peri / dorsolateral ento
	RSC	retrosplenial cortices
	Tu	olfactory tubercle
	Pir	piriform cortex
Rat subcortical regions	CPuD/CPuDM	caudate putamen - dorsal / dorsomedial
	CPuVL/CPuAM	caudate putamen - ventrolateral / anteromedial
	AcbSh	accumbens nucleus, shell
	SN	substantia nigra
	PrS/PaS	subiculum - pre / para
	DG	dentate gyrus
	Hipp-fi	hippocampus - fimbria
	CA	field CA1-3
	M	mamillary nucleus
	TS	triangular septal cunleus
	DS	dorsal subiculum
	BLA/MeA/CEA	amygdala - basolateral / medial / central
	SC / IC	colliculus - superior / inferior
	CERE/Crus2	cerebellum/ crus 2 of the ansiform lobule
	MS	medial septum nucleus
	PA	preoptic area
	ZI	thalamic nucleus - zona incerta
	VM/VL	thalamic nucleus - ventromedial / ventrolateral
Human subcortical regions	CERE	cerebellum
	GP	globus pallidus
	NA	nucleus accumbens
	SN	substantia nigra
	Brain Stem	brain stem
	Caudate	caudate nucleus
	Hippo	hippocampus
	TH	thalamus
	HTH	hypothalamus
	Amy	amygdala
	Pu	putamen

756
757

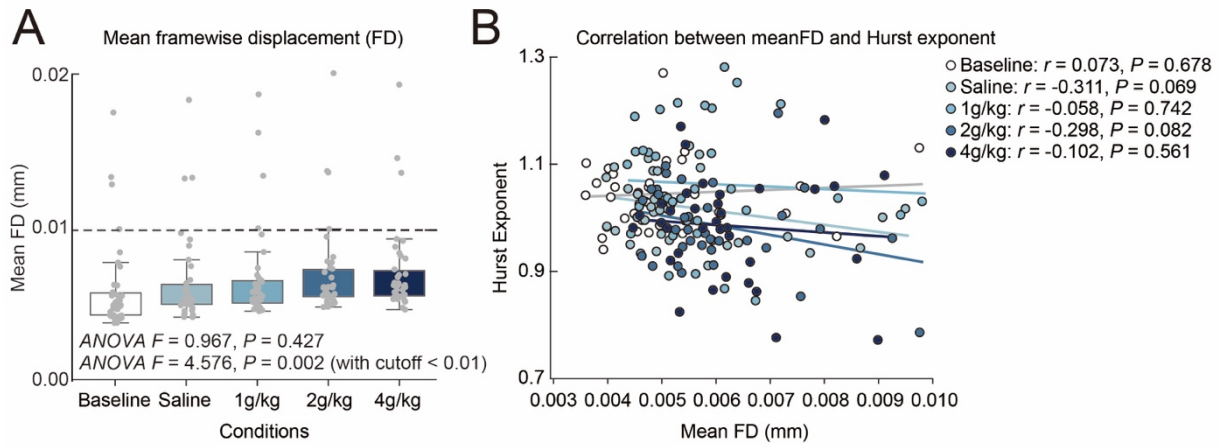

Supplementary Figure 1. Correlation between the Hurst exponent and motion in rats. (A) Mean framewise displacement (mean FD) for each condition in rats without a cutoff (ANOVA F = 0.967, P = 0.427) and with a cutoff of 0.01 mm (ANOVA F = 4.576, P = 0.002). The dashed line indicates a cutoff of 0.01 mm. **(B)** Correlation between mean FD and the Hurst exponent after applying the motion cutoff (0.1 mm). Baseline (white): r = -0.063, P = 0.709, Saline (cyan) : r = -0.075, P = 0.653, 1 g/kg (light blue): r = -0.023, P = 0.890, 2 g/kg (blue): r = -0.043, P = 0.800, 4 g/kg (dark blue): r = -0.002, P = 0.991).

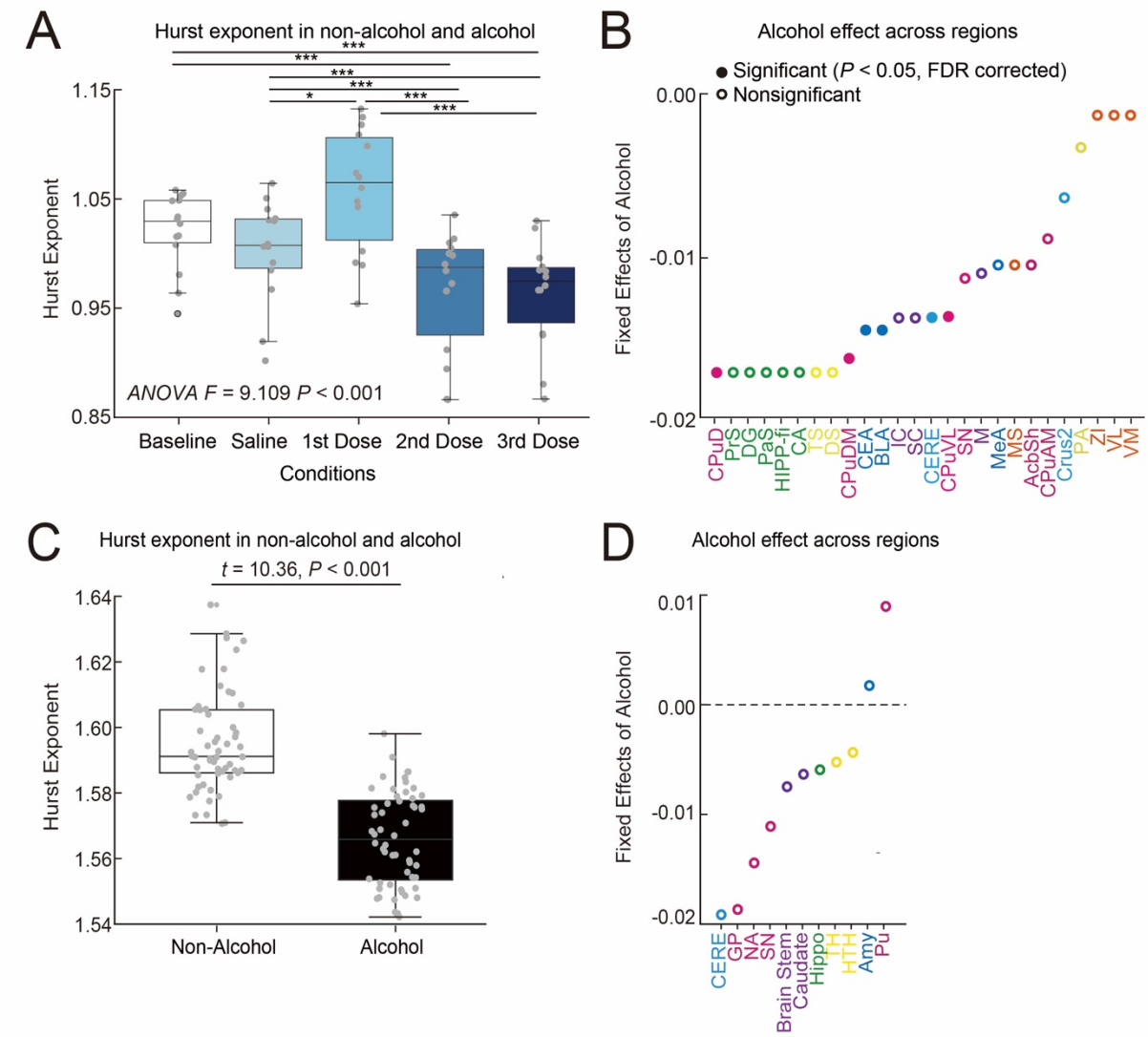

Supplementary Figure 2. Alcohol's effect on the Hurst exponent of subcortical regions. (A) The Hurst exponent averaged across subcortical regions in rats (ANOVA $F = 9.109$, $P < 0.001$). To control for motion, we regressed out the FD mean from the original Hurst values and added the residuals to the average Hurst exponent. Post-hoc Tukey HSD test $^{***}P < 0.001$, $^{**}P < 0.01$, $^{*}P < 0.05$. **(B)** Alcohol's effect across subcortical regions. Colored filled dots indicate regions with a significant alcohol effect that survived FDR correction, while unfilled dots represent regions with non-significant effects. Pink: Striatum, Green: Hippocampal, Yellow: Thalamic, Dark blue: Amygdala, Purple: Midbrain, Light blue: Cerebellum, Orange: Zonality. The full names of the regions are listed in Table S1. **(C)** The Hurst exponent averaged across subcortical regions in humans under non-alcohol (white) and alcohol (black) conditions ($t = 10.36$, $P < 0.001$). To control for motion, we regressed out the FD mean from the original Hurst values and added the residuals to the average Hurst exponent. **(D)** Alcohol's effect across subcortical regions in humans. Unfilled dots represent regions with non-significant effects. Pink: Striatum, Green: Hippocampal, Yellow: Thalamic, Dark blue: Amygdala, Purple: Midbrain, Light blue: Cerebellum. The full names of the regions are listed in Table S1.

761

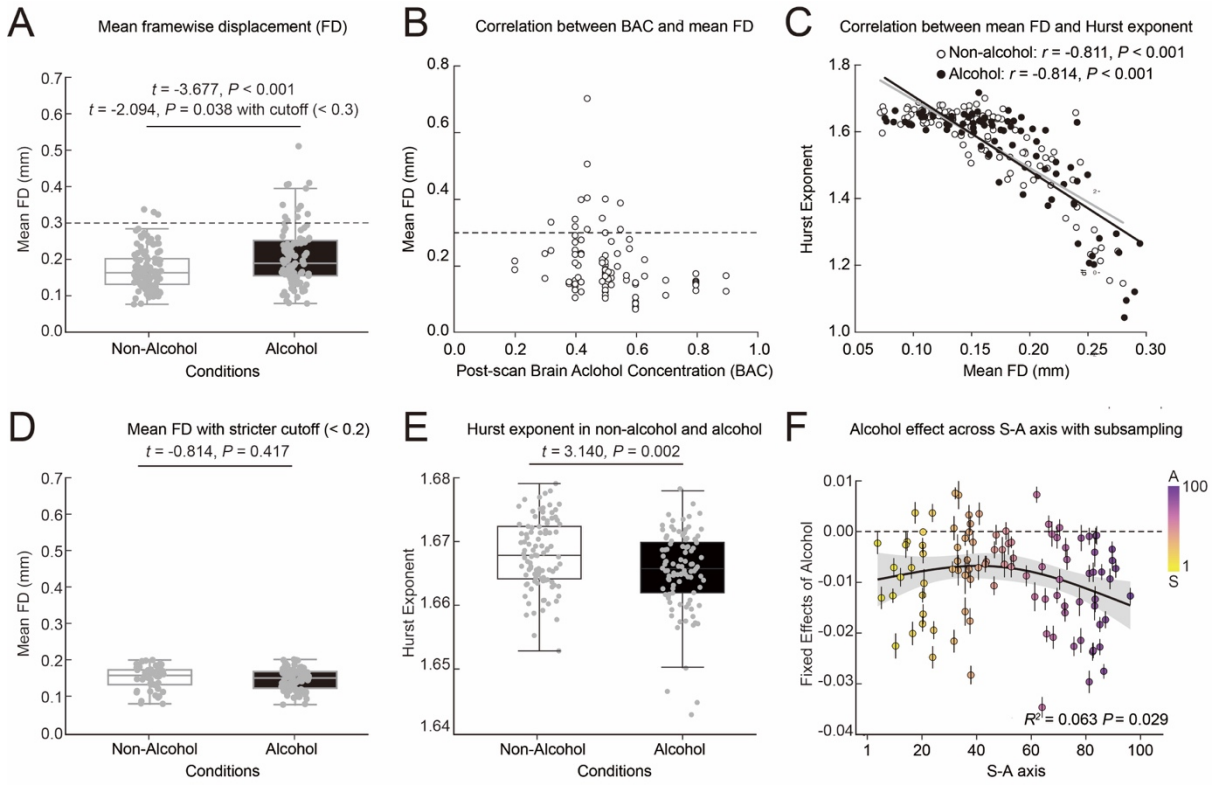

Supplementary Figure 3. Correlation between the Hurst exponent and motion in humans. (A) Mean framewise displacement (mean FD) in non-alcohol and alcohol conditions without a cutoff (t = -3.677, P < 0.001) and with a cutoff of 0.3 mm (t = -2.094, P = 0.038). The dashed line indicates a cutoff of 0.3 mm. **(B)** Correlation between post-scan blood alcohol content (BAC) and mean FD. The dashed line indicates a cutoff of 0.3 mm. **(C)** Correlation between mean FD and the Hurst exponent after apply the motion cutoff (0.3 mm). White dots represent non-alcohol sessions, and black dots represent alcohol sessions (Non-alcohol: r = -0.811, P < 0.001, Alcohol: r = -0.814, P < 0.001). **(D)** Mean framewise displacement (mean FD) in non-alcohol and alcohol conditions with a stricter cutoff of mean FD < 0.2 mm (t = -0.814, P = 0.417). **(E)** The whole-brain averaged Hurst exponent with a stricter cutoff (t = 3.140, P = 0.002). **(F)** Alcohol's effect across the cortex with balancing session counts between alcohol and non-alcohol conditions by subsampling the non-alcohol sessions (R^2 = 0.063, P = 0.029). The error bar represents the standard deviation across 10 subsamples.